

# Monopole oscillations in light nuclei with a molecular dynamics approach

T. Furuta,<sup>1</sup> K. H. O. Hasnaoui,<sup>2</sup> F. Gulminelli,<sup>1</sup> C. Leclercq,<sup>1</sup> and A. Ono<sup>2</sup>

<sup>1</sup> *LPC Caen (CNRS-IN2P3/ENSICAEN et Université), F-14050 Caen, France*

<sup>2</sup> *Department of Physics, Tohoku University, Sendai 980-8578, Japan*

Collective monopole vibrations are studied in the framework of an antisymmetrized version of molecular dynamics as a function of the vibration amplitude. The giant monopole resonance energy in  $^{40}\text{Ca}$  is sensitive to the incompressibility of the effective interaction, in good agreement with complete time-dependent Hartree-Fock calculations. The collective response of  $^{12}\text{C}$ ,  $^{16}\text{O}$ , and  $^{24}\text{Mg}$  is also studied. For these lighter nuclei that have an important contribution of an  $\alpha$ -clustered component, different frequencies are observed, corresponding to two different types of vibrations associated with breathing and moving of the underlying clusters. Possible connections with direct breakup into  $\alpha$  clusters at high excitation energy are discussed.

PACS numbers: 24.30.Cz, 21.65.-f, 24.30.Gd

## I. INTRODUCTION

Collective vibrations of nuclei are interesting phenomena in quantum many-body dynamics. The constituent nucleons coherently participate in these vibrations and the motion can be intuitively understood in classical terms as a global vibration of an excited liquid drop. In a quantum mechanical sense, the dynamics is described by a coherent superposition of many particle-hole excitations on top of the ground-state configuration. These collective vibrations have been experimentally observed for thirty years as broad resonances (giant resonances) in the high-energy spectrum of nuclei [1–4]. The existence of such resonances has been reported for many different medium-heavy and heavy nuclei in the isotopic table, and their characteristics have been successfully reproduced in mean-field-based approaches [5].

These theoretical studies have shown that collective modes are privileged probes of the effective interaction, and as such they can bear important information on nuclear matter properties. In particular, the isoscalar giant monopole resonance or the breathing mode of nuclei is connected to the incompressibility of nuclear matter, even if this connection is far from being direct [6, 7].

Experimental data on the isoscalar monopole response of nuclei as light as  $^{12}\text{C}$  or  $^{16}\text{O}$  [8–11] show a fragmented strength distribution, which is qualitatively understood as a global weakening of the collectivity but is not quantitatively understood. It is well known that correlations play an important role in the structure of these light nuclei and the application of standard Hartree-Fock (HF) or random phase approximation (RPA) calculations to their collective dynamics may be questionable. This is particularly true in nuclei presenting clustered structures, a phenomenon that is expected both in excited states and in the ground state of numerous light and medium-heavy  $N = Z$  nuclei [12, 13]. In such situations, one can expect that collective vibrations may imply collective motions of the underlying clusters. Indeed, it has already been reported in the literature that collective strengths to low-lying states are affected by the cluster degrees of

freedom [14, 15].

The giant monopole resonance (GMR) corresponds to relatively small amplitude of a collective monopole excitation. Another interesting regime of nuclear dynamics is given by large-amplitude collective motion with a significant compression of the system followed by expansion. At excitations of the order of 3 A MeV or higher, it leads to the observable phenomenon of nuclear fragmentation [16–19].

Here the situation is qualitatively similar to the excitation of giant resonances: When a heavy nucleus is compressed significantly, the dynamics of compression and expansion appears to be governed by global collective properties, namely, the nuclear matter equation of state, and appears to be largely independent of the structure properties of the excited nucleus [20, 21]. Conversely, if the ground state and/or excited states have pronounced clustered structure, one may expect an interplay between these structures and the collective dynamics and fragmentation pattern. A systematic study of the fragmentation of light clustered nuclei has never been done, but some indications exist as a preferential  $\alpha$ -particle emission from  $\alpha$ -structured nuclei [22–25].

In this respect, models able to describe both the small- and large-amplitude collective regime are useful tools for understanding collective nuclear dynamics. Interesting studies have been performed in the context of time-dependent Hartree-Fock (TDHF) calculations [26–34] and its semiclassical counterpart [35–38] and a cluster-based time-dependent approach [39–41].

Antisymmetrized versions of molecular dynamics models, antisymmetrized molecular dynamics (AMD) [42, 43] and fermionic molecular dynamics (FMD) [44], are powerful approaches for describing both nuclear structure and reactions. They are microscopic models based on nucleonic degrees of freedom. The wave function is modeled as a fully antisymmetrized product of Gaussian wave packets. The choice of the nonorthogonal Gaussian wave packets is a restriction of general Slater determinants, but it has an advantage of allowing spontaneous breaking of all spatial symmetries. Because of that, these models are particularly suitable to describe cluster and molecular

states. After projection over appropriate quantum numbers, they have been successfully applied to describe the structure change from shell-model-like structure to clustering structure [44–46]. They also have been applied to nuclear reactions from fusion [47] to multifragmentation reactions [42, 43, 48]. For small-amplitude collective modes, the isovector dipole oscillation has been studied with AMD [49] but almost no application to the isoscalar monopole modes has been performed to our knowledge.

In this paper, we use the simplest version of the model employing a single Slater determinant. This approximation is not sufficient to realistically describe nuclear spectroscopy, but it allows us to understand qualitatively the effect of clustering on the collective dynamics. The use of a fully time-dependent approach allows us in principle to study consistently the motion from the small-amplitude RPA regime to the large-amplitude fragmentation regime. In this first application, two-body collisions and quantum branching, which are necessary to explain experimental data of heavy-ion collisions around Fermi energies [42, 43, 48, 50], are not implemented, but their inclusion is straightforward.

The main difference between AMD and FMD concerns the width degree of freedom. In FMD, the centroids and width of Gaussians are both complex time-dependent variational parameters whereas, in AMD, the width is an external real number common to all the Gaussians. The isoscalar monopole oscillation is supposed to correspond to a breathing mode, so that the width degree of freedom may have a significant importance. By comparing the results between AMD and FMD, we would also like to clarify what degrees of freedom are important to properly describe compression modes.

## II. FORMALISM OF AMD AND FMD

In the AMD and FMD models, the optimal time dependence of the  $N$ -body wave function is obtained through the time-dependent variational principle

$$\delta \int_{t_1}^{t_2} \frac{\langle \Psi(t) | i\hbar \frac{d}{dt} - \hat{H} | \Psi(t) \rangle}{\langle \Psi(t) | \Psi(t) \rangle} dt = 0 \quad (1)$$

$$\delta |\Psi(t_1)\rangle = \delta |\Psi(t_2)\rangle = 0$$

within the constraint that  $|\Psi(t)\rangle$  is given by a Slater determinant of the single-particle states  $\psi$ ,

$$|\Psi\rangle = \frac{1}{\sqrt{A!}} \det_{ij} [\psi_i(j)], \quad (2)$$

where  $A$  is number of nucleons.

If no extra restriction on the single-particle wave functions  $\psi(\vec{r})$  is applied, Eq. (1) gives the TDHF equation [51]. However, in the AMD and FMD models, the single-particle wave functions  $\psi(\vec{r})$  are restricted to the Gaussian form:

$$\psi_i(\vec{r}) = \exp \left[ -\frac{1}{2a_i} (\vec{r} - \vec{b}_i)^2 \right] \chi_{\alpha_i} \quad (3)$$

where  $\vec{b}_i$  ( $i = 1, \dots, A$ ) are complex time-dependent variational parameters. In the FMD formulation, the wave packet width  $a_i$  is an additional complex time-dependent variational parameter. In contrast, in the AMD model, all wave packets share the same real constant width  $a_i = 1/2\nu = \text{const.}$  The spin-isospin states ( $\chi_{\alpha_i} = p \uparrow, p \downarrow, n \uparrow, n \downarrow$ ) give additional variational parameters, which are essential to describe charge-exchange reactions and spin excitations. In the present application to scalar-isoscalar collective modes, only spin and isospin saturated systems will be considered. We will then restrict ourselves to a simple variation in the configuration space and the spin-isospin states will be treated as constants of motion. The equations of motion for AMD and FMD as resulting from Eq. (1) can be written as

$$i\hbar \sum_{j\tau} C_{i\sigma,j\tau} \frac{dq_{j\tau}}{dt} = \frac{\partial \langle \hat{H} \rangle}{\partial q_{i\sigma}^*} \quad (4)$$

where  $\langle \hat{H} \rangle$  is the expectation value of the Hamiltonian  $\hat{H}$  taken with the wave function  $\Psi$ ,  $C_{i\sigma,j\tau}$  appears because of the non-orthogonality of Gaussian wave packets and is given by

$$C_{i\sigma,j\tau} = \frac{\partial^2}{\partial q_{i\sigma}^* \partial q_{j\tau}} \ln \langle \Psi | \Psi \rangle, \quad (5)$$

and  $q_{i\sigma}$  give the variational parameters for nucleon  $i$  in the model, namely,  $q_{i\sigma=1,\dots,4} = a_i, b_{ix}, b_{iy}, b_{iz}$  in FMD and  $q_{i\sigma=1,\dots,3} = b_{ix}, b_{iy}, b_{iz}$  in AMD. For further details, see Refs. [44, 48].

## III. DESCRIPTION OF GROUND-STATE PROPERTIES

The ground state is obtained by minimizing the energy expectation value  $\langle \hat{H} \rangle \equiv \langle \Psi | \hat{H} | \Psi \rangle / \langle \Psi | \Psi \rangle$  with respect to the variational parameters of the models.

The molecular dynamics ansatz Eq. (3) represents a restriction of the full space for the single-particle wave function. This means that a full HF calculation in three-dimensional  $\mathbf{r}$ -space is a generalization of this model, though molecular dynamics can be superior to HF if the latter is solved on a truncated basis or by imposing the conservation of chosen spatial symmetries [52]. As a consequence, AMD and FMD ground-state energies have to be seen as upper limits of the HF ground-state value.

Table I shows some ground-state properties, namely, the ground-state energy  $E_{\text{g.s.}}$  and the matter root-mean-square radius  $R_m$  obtained by AMD and FMD for several selected nuclei. Results with SLy4 [53], Gogny [54], and the old SIII effective interaction [55] are shown. SLy4 and SIII are Skyrme interactions, namely, of  $\delta$ -type, with symmetric nuclear matter incompressibilities of  $K_\infty = 230$  MeV and  $K_\infty = 355$  MeV, respectively. Gogny is a finite-range interaction with an incompressibility modulus of  $K_\infty = 228$  MeV. Both Gogny and

SLy4 are realistic interactions that have been successfully compared to different experimental data on nuclear masses and collective modes. SIII also gives reasonable values for nuclear masses along the stability valley, but it is known to exhibit a too high incompressibility. The results of a three-dimensional HF calculation with SLy4 using the code of Ref. [52] and the experimental data from the Atomic Mass Evaluation [56] are also shown in the table for comparison.

		AMD			FMD		HF	Exp
		SLy4	SIII	Gogny	SLy4	SIII	SLy4	
$^4\text{He}$	$E_{\text{g.s.}}$	-26.0	-25.6	-28.9	-26.2	-25.5	-26.7	-28.3
	$R_m$	1.73	1.69	1.63	1.73	1.69	1.96	
$^{12}\text{C}$	$E_{\text{g.s.}}$	-72.2	-70.6	-74.9	-77.4	-75.2	-90.7	-92.2
	$R_m$	2.57	2.53	2.52	2.57	2.51	2.44	
$^{16}\text{O}$	$E_{\text{g.s.}}$	-121.5	-120.4	-125.3	-127.9	-125.4	-128.6	-127.6
	$R_m$	2.63	2.59	2.58	2.63	2.60	2.67	
$^{40}\text{Ca}$	$E_{\text{g.s.}}$	-330.6	-322.1	-334.2	-338.9	-330.3	-344.6	-342.1
	$R_m$	3.40	3.42	3.36	3.40	3.41	3.39	

TABLE I: Ground-state properties [energy  $E_{\text{g.s.}}$  (MeV) and root-mean-square radius  $R_m$  (fm)] for  $^4\text{He}$ ,  $^{12}\text{C}$ ,  $^{16}\text{O}$  and  $^{40}\text{Ca}$  calculated by AMD and FMD with three different effective interactions (SLy4, SIII, and Gogny). Calculation results of the HF method with SLy4 using the code of Ref. [52] and experimental data (EXP.) from the Atomic Mass Evaluation [56] are also shown in the table for comparison.

AMD $\nu_{\text{g.s.}}$	SLy4	SIII	Gogny
$^4\text{He}$	0.19	0.20	0.21
$^{12}\text{C}$	0.155	0.16	0.16
$^{16}\text{O}$	0.155	0.16	0.16
$^{40}\text{Ca}$	0.125	0.125	0.13

TABLE II: List of the inverse width optimal value  $\nu_{\text{g.s.}}$  ( $\text{fm}^{-2}$ ) for the AMD calculations.

In AMD calculations, the inverse width  $\nu$  is an external parameter optimized for each nucleus to ensure a minimum  $\langle \hat{H} \rangle$ . The optimal values  $\nu_{\text{g.s.}}$  are listed in Table II. The main difference between AMD and FMD in this context, therefore, is that (i) AMD takes a common width for all the Gaussians whereas FMD can take a different width for each Gaussian and (ii) the imaginary part of the width is an extra variational parameter for FMD whereas it is fixed to zero in AMD. In actual applications, point (i) is the most important since it helps in describing neutron skins and neutrons halos [57–59]. However, the imaginary parts of the variational parameters turn out to be very close to zero in FMD ground states, even if they can play a role in the dynamical evolution.

As was already observed in previous more systematic studies [44, 48], the overall experimental features of the

ground-state properties are reproduced by both AMD and FMD. The difference between the results of HF and those of AMD and FMD is not significant for most of the cases, even though the state  $|\Psi\rangle$  in AMD and FMD does not cover the whole possible range of Slater determinants. This result shows that the Gaussian ansatz has a high degree of flexibility, at least as far as the shown observables are concerned.

The only exception is given by the case of  $^{12}\text{C}$ , which is significantly underbound by both AMD and FMD. This discrepancy is not due to the limited variational space of the spatial wave functions, but rather to the lack of the spin-orbit interaction, which has been neglected in the present work. In fact, if we switch off the spin-orbit interaction in the HF calculation, we obtain  $E_{\text{g.s.}} = -74.8$  MeV, which is close to the FMD result. This value is slightly higher than the FMD result, which may be due to the mirror symmetry in  $xyz$  axes imposed on the single-particle wave functions in the HF calculation [52]. To properly introduce the spin-orbit interaction into FMD (and AMD), the variation of the spin wave function together with the configuration wave function [44], as well as the angular momentum projection, would be necessary [57–60]. These features are essential for a quantitative study of nuclear structure and spectroscopy, but they are not expected to play an important role in the study of the monopole oscillation.

Because of the restriction of the accessible configuration space in molecular dynamics models, the following relation is expected among the ground-state energies calculated by these models if the same effective interaction is used:

$$E_{\text{g.s.}}(\text{HF}) \leq E_{\text{g.s.}}(\text{FMD}) \leq E_{\text{g.s.}}(\text{AMD}). \quad (6)$$

However, this inequality is not systematically observed. This is due to the different treatment of the spurious zero-point kinetic energy of the center-of-mass motion  $T_{\text{zero}}$ . It is well known that the center-of-mass motion gives rise to a spurious contribution in HF-based models, owing to the breaking of translational invariance. The first-order contribution can be subtracted by replacing the kinetic part of the Hamiltonian  $\hat{H}_{\text{kin}} = \frac{1}{2m} \sum_{i=1}^A \hat{p}_i^2$  with

$$\begin{aligned} \hat{H}_{\text{kin}} &- \frac{1}{2mA} \left( \sum_{i=1}^A \hat{p}_i \right)^2 \\ &= \hat{H}_{\text{kin}} - \frac{1}{2mA} \left( \sum_{i=1}^A \hat{p}_i^2 + \sum_{i \neq j=1}^A \hat{p}_i \cdot \hat{p}_j \right), \end{aligned} \quad (7)$$

where  $m$  is the mass of the nucleon. The one-body term is readily implemented by multiplying a factor  $(1 - 1/A)$  to the kinetic energy. The two-body term is numerically expensive, and it is neglected both in the standard choice of HF [52] and in our FMD calculations. Conversely, in AMD, the center-of-mass coordinate can be separated from the intrinsic degrees of freedom and there is no

spurious coupling between them. Therefore, the contribution of the spurious center-of-mass motion is readily calculated as

$$T_{\text{zero}} = \frac{1}{2mA} \frac{\langle \Psi_{\text{AMD}} | (\sum_{i=1}^A \hat{p}_i)^2 | \Psi_{\text{AMD}} \rangle}{\langle \Psi_{\text{AMD}} | \Psi_{\text{AMD}} \rangle} = \frac{3\hbar^2\nu}{2m} \quad (8)$$

and can be exactly subtracted from the AMD ground-state energy. This approximate treatment of the center-of-mass motion in HF and FMD can be of some importance in the case of the light nuclei considered here. When employing in the AMD calculation the same approximate treatment of the center-of-mass motion that is currently used in FMD and HF, we have verified that indeed  $E_{\text{g.s.}}(\text{HF}) \leq E_{\text{g.s.}}(\text{FMD}) \leq E_{\text{g.s.}}(\text{AMD})$  is always found.

#### IV. DESCRIPTION OF THE ISOSCALAR MONOPOLE COLLECTIVE MOTION

Collective motions are easily identified in time-dependent approaches as periodic oscillations of the associated collective variables. For  $L = 0$  excitations, an initial perturbation preserving radial symmetry induces a collective vibration of the nucleus with specific frequencies that can be extracted from a Fourier analysis of the oscillation pattern. The collective vibration of a spherical nucleus in small amplitude is typically associated with a unique frequency, the giant monopole resonance, whose energy is directly related to the second derivative of the energy functional with respect to the root-mean-square radius, that is, to the nucleus incompressibility coefficient [5].

The advantage of explicit time-dependent approaches compared to the more standard RPA analysis is that they allow multiple excitations of giant resonance and coupling to more complex high-energy channels [36, 37]. Since at large amplitude the monopole oscillation evolves toward radial expansion followed by nuclear multifragmentation, we may expect a correlation between the oscillation frequencies and the expansion speed which may affect the fragmentation pattern [61]. In the standard time-dependent treatment of collective excitations [26, 62, 63], the initial state  $|\Psi(t=0)\rangle$  is prepared by applying the generator of the collective excitation under study,  $\hat{U}_0(k) = \exp(ik\hat{Q}_n)$ , on the ground-state wave function  $\langle \vec{r}_1, \dots, \vec{r}_A | 0 \rangle$ , where  $\hat{Q}_0 = \hat{r}^2$  for the isoscalar monopole. In this case the Fourier transform of the temporal variation of the collective response  $\Delta\sqrt{\langle \hat{r}^2 \rangle} = \sqrt{\langle \hat{r}^2 \rangle(t)} - \sqrt{\langle \hat{r}^2 \rangle(t=0)}$ ,

$$\text{FT}[r](\omega) = \int_{-\infty}^{\infty} dt \Delta\sqrt{\langle \hat{r}^2 \rangle(t)} e^{-i\omega t} \quad (9)$$

in the small-amplitude limit ( $k \rightarrow 0$ ) is directly propor-

tional to the strength function

$$\Im(\text{FT}[r](\omega)) \propto S(\omega) = \sum_n |\langle 0 | \hat{r}^2 | n \rangle|^2 \delta(\hbar\omega - E_n), \quad (10)$$

meaning that the excitation probability of the different frequencies is a direct measure of the transition probability to the excited states  $|n\rangle$  of energy  $E_n$ , induced by the excitation operator  $\hat{Q}_0$ .

This treatment cannot be applied to the AMD model. Indeed the application of the monopole operator  $\hat{U}_0(k)$  to the single-particle wave function, Eq. (3), produces a new Gaussian state with centroid  $\vec{b}'_i$  and width  $a'_i$ :

$$\vec{b}'_i = \frac{1 + 2ika_i^*}{1 + 4k^2|a_i|^2} \vec{b}_i ; \quad a'_i = \frac{1 + 2ika_i^*}{1 + 4k^2|a_i|^2} a_i \quad (11)$$

which, because of the nonzero imaginary part of the width, does not belong to the AMD variational space. This simple observation already suggests that the dynamical evolution of the width may play a significant role in the breathing mode.

However, we can still study compressional collective modes in AMD by choosing the initial state as a common translation in the radial direction of the Gaussian centroids with respect to their ground-state value,

$$\begin{aligned} \Re(\vec{b}_i(t=0)) &= (1 + \lambda)\Re(\vec{b}_i^0) \\ \Im(\vec{b}_i(t=0)) &= \Im(\vec{b}_i^0). \end{aligned} \quad (12)$$

This initial state, as any other modifying the root-mean-square radius of the nucleus, will excite the same monopole eigenmode as the application of the monopole boost  $\hat{U}_0(k)$  [33]. This is however not true as far as the spectral function  $\text{FT}[r](\omega)$  is concerned. Indeed in the case of the AMD model where the Gaussian centroids are the only variational parameters, this initial state corresponds to minimizing the total energy in the presence of a perturbative external field  $-\lambda r^2$  for some chosen values of  $\lambda$ . It is possible to show [26, 62] that including an external harmonic field  $V_{\text{ext}} = \lambda \hat{r}^2 \theta(-t)$  in the TDHF dynamics is indeed an alternative way to prepare the initial monopole state. Such an initial condition produces in the linear response regime a spectral function different from Eq. (10), where the probability of the different collective states is weighted by the inverse of the state energy.

For this reason we will concentrate on the energy of the collective states, which appears to be independent of the chosen initial condition, rather than on the detailed shape of the strength function. Another argument for that is given by the fact that a realistic description of the strength function and the associated energy weighted sum rule (EWSR) requires a proper treatment of the damping of collective motion, which in turn demands the inclusion of higher order correlations in the form of collisions and branching [48]. Finally, since the equations of motion of AMD and FMD are obtained by restricting



the TDHF single-particle wave functions to Gaussians, the strength function obtained by AMD or FMD will approximately satisfy the corresponding RPA sum rule only if the restriction on the single-particle wave functions is not critical. All these difficulties are much less critical as far as the frequencies are concerned. For all the cases presented in this paper, the time evolution of the root-mean-square nuclear radius presents only a few well-distinct frequencies, meaning that the collective energies can always be unambiguously recognized.

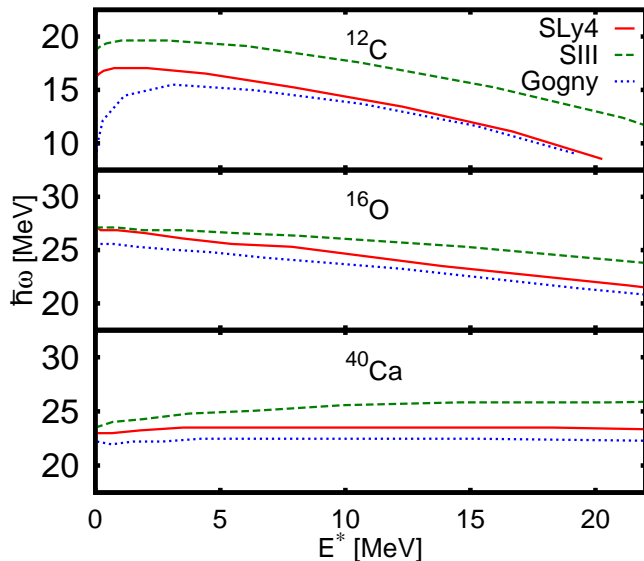


FIG. 1: (Color online) AMD prediction for the frequency  $\hbar\omega$  of the monopole oscillation as a function of the oscillation energy for  $^{12}\text{C}$ ,  $^{16}\text{O}$ , and  $^{40}\text{Ca}$  with the SLy4, SIII, and Gogny interactions.

In AMD calculations for monopole oscillations of  $^{12}\text{C}$ ,  $^{16}\text{O}$ , and  $^{40}\text{Ca}$ , the spectral function  $\text{FT}[r](\omega)$  shows only a single peak and thus a single frequency in the oscillation. The peak frequency  $\hbar\omega$  as a function of oscillation excitation energy, which is directly related to the oscillation amplitude, with the three different interactions (SLy4, SIII and Gogny) are shown in Fig. 1. A global independence of the peak frequency on the excitation energy is observed in the case of  $^{40}\text{Ca}$ , whereas the peak frequency gradually decreases for  $^{12}\text{C}$  and  $^{16}\text{O}$  at high excitation energies ( $>5$  MeV). For low excitation energy (small-amplitude) oscillations ( $<5$  MeV), the peak frequency varies abruptly as a function of excitation energy for the  $^{12}\text{C}$  case if the Gogny interaction is used. A clear, even if much less spectacular, frequency change for small amplitude oscillations is also observed for the other effective interactions and the other nuclei. This behavior will be discussed in detail in the next section. However, this behavior at small amplitudes is not likely to strongly affect the energy of one-phonon states when the collective motion is quantized. The physical frequency that is relevant to the breathing mode is rather the one at the

excitation energy of the mode itself, since the percentage of the one-phonon state is maximized at this energy.

For the case of  $^{40}\text{Ca}$ , different theoretical studies exist on the GMR in this nucleus [32, 64], which can thus be considered as a benchmark for our calculations. The ground state of  $^{40}\text{Ca}$  is obtained in AMD as a structureless spherical distribution of neutron and proton densities. The resulting monopole peak is found at an energy  $\hbar\omega$  in reasonably good agreement with TDHF [32] ( $\hbar\omega = 22.1$  MeV) and RPA [64] ( $\hbar\omega = 21.5$  MeV) calculations using the same SLy4 effective interaction.

The SIII interaction is employed here for the purpose of exploring the sensitivity of the monopole response to the nuclear matter properties. As expected, as the incompressibility  $K_\infty$  increases from 230 MeV (SLy4) to 355 MeV (SIII), all the peak frequencies increase, showing that indeed collective compression and expansion can be addressed in molecular-dynamics-based formalisms.

The peaks obtained by AMD turn out to be without a physical width ( $\delta$ -function-like). In principle the energy of the modes is above the threshold of particle emission and the motion should be damped by the coupling to the continuum [26, 28, 32]. This is however not observed in the simulation, showing that the AMD wave function ansatz is not flexible enough to properly describe particle evaporation. The inclusion of higher order correlations is also required for a proper treatment of the damping of collective motions. In future studies it would be interesting to investigate whether the AMD models are able to reproduce the width of the collective resonances by introducing the two-body collisions and quantum branching [48].

## V. DIFFERENT MODES AND THE ROLE OF THE WIDTH

In AMD calculations, the inverse width parameter  $\nu$  is an external parameter and the calculations shown in Sec. IV were performed using the optimal value  $\nu_{\text{g.s.}}$  (table II), namely, the one that gives a minimum ground-state energy. However, there is no strong reason to adopt  $\nu_{\text{g.s.}}$  for the oscillation calculation if the collective excited states have considerably different structure from the ground state. For example, if the collective excited states have a strong clustered structure, the optimal choice of  $\nu$  for individual clusters may be more suitable than  $\nu_{\text{g.s.}}$ . Furthermore, in some applications of AMD such as to nuclear matter and heavy-ion reactions, it is not practical to adjust  $\nu$  for individual nuclei that appear in the system. For these reasons, it is important to understand how the characters of monopole oscillation depend or do not depend on the choice of  $\nu$ , which we will study in this section. We take the  $^{12}\text{C}$  calculation as a reference in the following, but qualitatively similar results are observed for  $^{16}\text{O}$  and  $^{24}\text{Mg}$ .

Figure 2 shows the position of the peak frequency in the spectral function  $\text{FT}[r](\omega)$  of  $^{12}\text{C}$  by AMD with SLy4

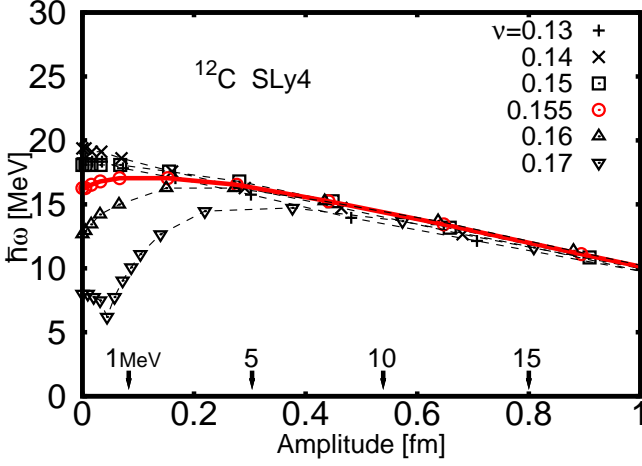


FIG. 2: (Color online) AMD prediction for the peak position  $\hbar\omega$  of the monopole oscillation for  $^{12}\text{C}$  with the SLy4 interaction as a function of the oscillation amplitude for different values of the inverse width parameter  $\nu$  ( $\text{fm}^{-2}$ ). The excitation energies corresponding to oscillation amplitudes in the case of the optimal width  $\nu = 0.155 \text{ fm}^{-2}$  (full line) are indicated by arrows.

as a function of oscillation amplitude for different inverse width parameters  $\nu$ . The full line shows the result of the ground state optimal width ( $\nu_{\text{g.s.}} = 0.155 \text{ fm}^{-2}$ ). The excitation energies corresponding to oscillation amplitudes for this line are also indicated in the figure.

In the region of the amplitude greater than 0.4 fm, different choices of  $\nu$  give almost identical oscillation frequencies, and in particular the prediction of GMR energy is almost independent of the choice of  $\nu$ . The frequency gradually decreases as the amplitude increases. This behavior can be physically understood, since above the breakup threshold the expansion can be followed by a breakup of the system and not by a recompression, corresponding to an oscillation period that tends to diverge (that is, a frequency that tends to zero).

In small-amplitude oscillations ( $< 0.4 \text{ fm}$ ), the oscillation frequency varies abruptly as a function of the amplitude for some choices of  $\nu$ . A very peculiar behavior is observed in particular for the case  $\nu = 0.17 \text{ fm}^{-2}$  in the small-amplitude regime. With this choice of the width parameter the monopole frequency shows a well-pronounced minimum at a specific value of the oscillation amplitude (0.04 fm). In the following we will show that this is due to the presence of two possible distinct oscillation regimes in the AMD dynamics by investigating the motion of wave packet centroids.

The motion of Gaussian centroids gives some useful information on the time evolution of the system, though the centroids do not correspond to the physical positions of nucleons owing to antisymmetrization. In the AMD dynamics of  $^{12}\text{C}$ , three ensembles of four Gaussians with different spin-isospin ( $p \uparrow$ ,  $p \downarrow$ ,  $n \uparrow$ , and  $n \downarrow$ ) take al-

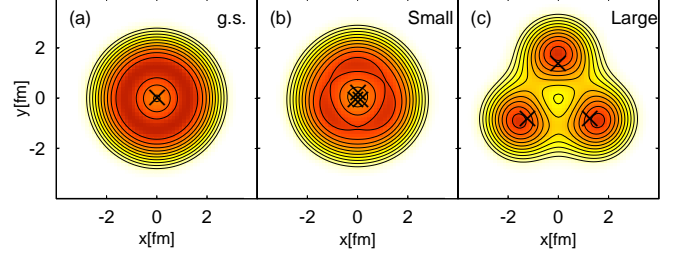


FIG. 3: (Color online) AMD density distributions of  $^{12}\text{C}$  with the SLy4 interaction projected on the plane perpendicular to the symmetry axis ( $x$ - $y$  plane) for (a) the ground state and the maximum amplitude stage of the monopole vibration at (b)  $E^* = 0.1 \text{ MeV}$  and at (c)  $E^* = 5 \text{ MeV}$ . The cross marks in the figures indicate the parameter positions of the effective “ $\alpha$ ”s (See text).

most the same time-dependent value for their  $\vec{b}$  parameter. The global  $^{12}\text{C}$  configuration shows therefore a “3- $\alpha$ -triangular” structure during the time evolution. The density distribution does not show spatial clustered structure at very small amplitude [Fig. 3(b)] because of the large overlap among the “ $\alpha$ ”s and the antisymmetrization effect among the nucleons, but these structures are clearly visible for larger amplitude vibrations [Fig. 3(c)]. We will speak of effective “ $\alpha$ ”s in the following, where the word “effective” means that the associated four nucleons do not form three independent  $\alpha$  particles because of the global antisymmetrization of the wave function.

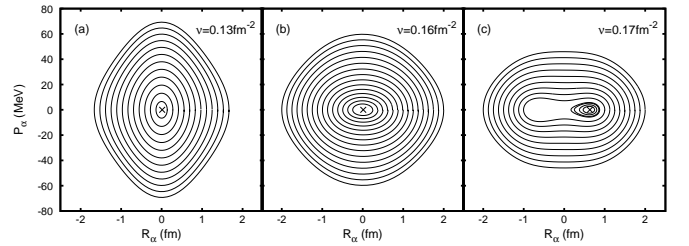


FIG. 4: Phase-space trajectory of the AMD monopole oscillation of  $^{12}\text{C}$  from the evolution of the variational parameters of one “ $\alpha$ ” (see text) for (a)  $\nu = 0.13 \text{ fm}^{-2}$ , (b)  $0.16 \text{ fm}^{-2}$ , and (c)  $0.17 \text{ fm}^{-2}$  with SLy4. Each contour corresponds to a different initial expansion, the largest circle being associated with the largest amplitude oscillation. The global oscillation pattern of  $^{12}\text{C}$  can be deduced from symmetry considerations (see text).

The active degrees of freedom in this motion are the variational parameters of one of these effective “ $\alpha$ ”s in

$^{12}\text{C}$ , namely, the Gaussian centroid parameters

$$\begin{aligned}\vec{R}_\alpha &= \frac{1}{4} \langle \Phi_\alpha | \hat{r} | \Phi_\alpha \rangle = \frac{1}{4} \sum_{i=1}^4 \Re(\vec{b}_i) \\ \vec{P}_\alpha &= \langle \Phi_\alpha | \hat{p} | \Phi_\alpha \rangle = 2\hbar\nu \sum_{i=1}^4 \Im(\vec{b}_i); \end{aligned} \quad (13)$$

the other two effective “ $\alpha$ ”s move in phase to keep the triangular symmetry owing to the symmetry of the excitation.  $\vec{R}_\alpha = R_\alpha \vec{u}_r$  and  $\vec{P}_\alpha = P_\alpha \vec{u}_r$  oscillate along the radial direction  $\vec{u}_r = \vec{R}_\alpha(t=0)/|\vec{R}_\alpha(t=0)|$ . The trajectories of  $R_\alpha$  and  $P_\alpha$  for three different choices of the inverse width are shown in Fig. 4. The ground-state ( $R_\alpha, P_\alpha$ ) values are indicated by the crosses in Fig. 4. In the case of a wide Gaussian width  $\nu = 0.13 \text{ fm}^{-2}$  [Fig. 4(a)] the position of the effective “ $\alpha$ ”s in the ground state coincides with the center of mass of the nucleus. The trajectories circulate in phase space around  $(R, P) = (0, 0)$  and the other two effective “ $\alpha$ ”s move in phase so that this motion corresponds to the crossing of “3- $\alpha$ ” as schematically shown by the cartoon of Fig. 5(a). For narrower Gaus-

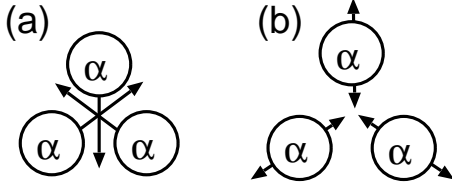


FIG. 5: Schematic representation of the two possible oscillation regimes observed in AMD calculations varying the Gaussian width and/or the motion amplitude.

sian width  $\nu > 0.16 \text{ fm}^{-2}$ , the ground state  $R_\alpha$  becomes finite, indicating an explicit “ $\alpha$ ” structure even in the ground state. In this case the small-amplitude oscillations [Fig. 4(c)] correspond to vibrations around this finite value, leading to a trajectory confined to the positive  $R_\alpha$ -coordinate space. This motion can be visualized as three effective “ $\alpha$ ”s oscillating around their ground state values as schematically indicated by Fig. 5(b). Increasing the excitation energy, and therefore increasing the amplitude of the motion, we find trajectories circulating around  $(R_\alpha, P_\alpha) = (0, 0)$  as in the case of  $\nu = 0.13 \text{ fm}^{-2}$ . The frequency minimum for  $\nu = 0.17 \text{ fm}^{-2}$  in Fig. 2 is observed at the transition between these different oscillation regimes. The small-amplitude oscillations observed with  $\nu = 0.16 \text{ fm}^{-2}$  [Fig. 4(b)] are located at the transition between the two motions, which explains the strong  $\nu$  dependence of the peak frequency for the small amplitude oscillations in Fig. 2.

As the time-dependent state  $|\Psi_{\text{AMD}}[q(t)]\rangle$  violates the symmetries, a more desirable approach is to apply the time-dependent variational principle to the state  $P(0^+)|\Psi_{\text{AMD}}[q]\rangle$  after the parity and angular momentum projection. For the oscillations with two regimes

as in Fig. 4(c), the excitation from the ground state, which has a finite “ $\alpha$ ” clustering, should couple to the excitation from the parity-reflected ground state. The lack of such a coupling in the present calculation may be a reason of the low oscillation frequency around the transitional situation between Figs. 5(a) and 5(b). However, if the oscillation amplitude is large (namely, if the “deformation” of the intrinsic state  $|\Psi_{\text{AMD}}[q(t)]\rangle$  is large enough), we can expect that the effect of the parity and angular momentum projection is not so important. It should also be noted that a kind of many-particle many-hole excitations (namely, cluster excitation) is included in the one-phonon state of the oscillation if it is extracted from the time-dependent many-body state  $|\Psi_{\text{AMD}}[q(t)]\rangle$  or  $P(0^+)|\Psi_{\text{AMD}}[q(t)]\rangle$  around the GMR amplitude.

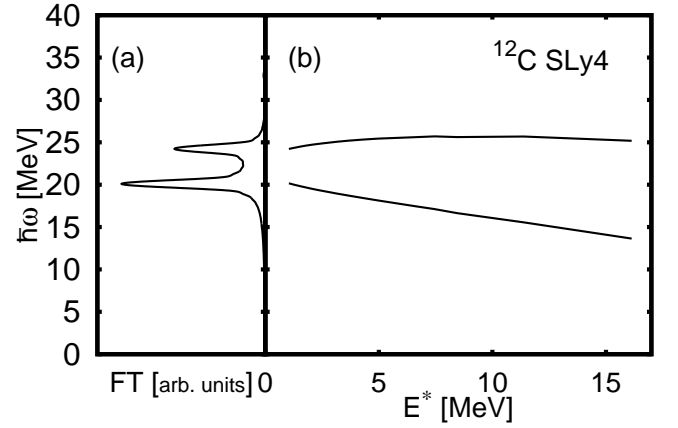


FIG. 6: (a) The spectral function  $\text{FT}[r](\omega)$  in arbitrary units of the FMD monopole oscillation in small amplitude for  $^{12}\text{C}$  with the SLy4 interaction, obtained by the same initial state as in the AMD calculation. (b) The peak position  $\hbar\omega$  as a function of the oscillation amplitude.

From these discussions, it is very interesting to see the results of FMD, which explores dynamically the different values of wave packet widths  $\{a\}$  as well as the centroids  $\{\vec{b}\}$ . Figure 6 shows the position of the peak frequency  $\hbar\omega$  in the spectral function  $\text{FT}[r](\omega)$  of  $^{12}\text{C}$  by FMD as a function of oscillation energy, where the initial state is prepared by Eq. (12). The spectral function in small amplitude is shown on the left side of this figure. The widths of the peaks are only a numerical artifact coming from the time filter [28], which is applied to compensate for the finite integration time in the Fourier transform. In the case of FMD, there are two peaks in the spectral function of  $^{12}\text{C}$  and the two lines in Fig. 6(b) correspond to the frequencies of these peaks. The behavior of the lower frequency follows closely the behavior of the one observed in AMD in the excitation energy regime where no sensitivity to the width was observed. However, a smooth behavior is also obtained at the lowest amplitude, showing that indeed two types of vibrations could be physically present.

For comparison, the experimental monopole strength

distribution [9] shows a fragmented structure composed of at least four different peaks between 13 and 45 MeV of excitation energy exhausting around 27% of the EWSR. The average energy in this excitation energy range is  $m_1/m_0 = 21.9$  MeV with an root-mean-square width of 4.8 MeV, in qualitative but not quantitative agreement with our results. The experimental data also show a low-energy peak that is associated with the excitation of the Hoyle state. No strength at these low energies is observed in our calculation, consistent with the fact that effects beyond mean field have been shown to be necessary to correctly reproduce the Hoyle state [13, 46].

To understand the physical meaning of the two peaks observed in the calculation, let us investigate the dynamics of variational parameters of  $^{12}\text{C}$  in the model. Similar to the case of AMD, three ensembles of four Gaussians with different spin-isospin ( $p \uparrow$ ,  $p \downarrow$ ,  $n \uparrow$ , and  $n \downarrow$ ) take almost the same time-dependent values for their  $\vec{b}$  parameters and constitute a “3- $\alpha$ -triangular” structure. The  $a$  parameters associated with each of the three “ $\alpha$ ”s oscillate in the same way. Therefore, the active degrees of freedom in the FMD motion are given by the centroid of the “ $\alpha$ ”s like in AMD,

$$\begin{aligned}\vec{R}_\alpha &= \frac{1}{4} \langle \Phi_\alpha | \hat{r} | \Phi_\alpha \rangle = \frac{1}{4} \sum_{i=1}^4 \left\{ \Re(\vec{b}_i) + \frac{\Im(a_i) \Im(\vec{b}_i)}{\Re(a_i)} \right\} \\ \vec{P}_\alpha &= \langle \Phi_\alpha | \hat{p} | \Phi_\alpha \rangle = \hbar \sum_{i=1}^4 \frac{\Im(\vec{b}_i)}{\Re(a_i)}\end{aligned}\quad (14)$$

together with the width of the effective “ $\alpha$ ”s,

$$\begin{aligned}\sigma_R &= \langle \Phi_\alpha | \hat{r}^2 | \Phi_\alpha \rangle = \sum_{i=1}^4 \frac{3|a_i|^2}{2\Re(a_i)} \\ \sigma_P &= \langle \Phi_\alpha | \hat{p}^2 | \Phi_\alpha \rangle = \sum_{i=1}^4 \frac{3\hbar^2}{2\Re(a_i)}.\end{aligned}\quad (15)$$

Figure 7 shows the oscillation frequencies associated with these different observables. We can see that the first peak present in the monopole response (Fig. 6) is associated with the time variation of the centroid of “ $\alpha$ ”  $R_\alpha$ . This physically corresponds to an oscillation of the positions of three “ $\alpha$ ” clusters around the center of the nucleus [see Fig. 4(a) and Fig. 5(a)]. In the absence of the width degree of freedom, this is the only collective monopole motion accessible to the system, and this is why the AMD response contains a single peak. The prediction of AMD and FMD concerning this peak is in good agreement because it comes out that  $\Im(a) \sim 0$  during the whole dynamical evolution.

The second peak at higher energy observed in the monopole response (Fig. 6) is associated with the time variation of the widths. It is physically associated with the coherent vibration of the constituting “ $\alpha$ ” clusters, as shown by the fact that this frequency appears in the Fourier transform  $\sigma_R(t)$ . This mode is very similar to the

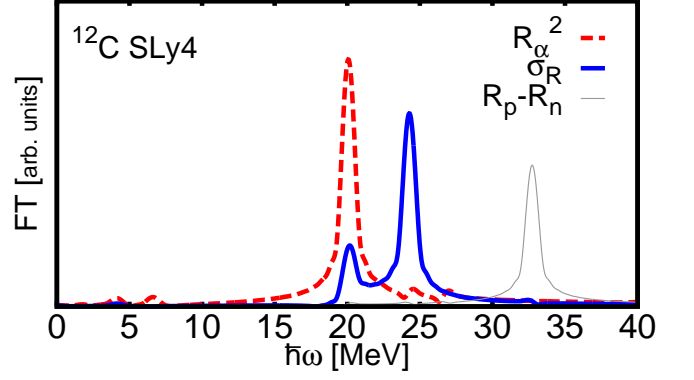


FIG. 7: (Color online) Fourier transforms in arbitrary units of FMD monopole oscillations ( $^{12}\text{C}$  with the SLy4 interaction) associated with the square of the position of the effective “ $\alpha$ ” from the  $^{12}\text{C}$  center of mass  $R_\alpha^2(t)$  (dashed line); the coordinate width of the effective “ $\alpha$ ”  $\sigma_R(t)$  (thick line); the differential time evolution of the proton and neutron for square radius ( $R_{\text{proton}} - R_{\text{neutron}}$ ) (thin line).

standard breathing mode of medium-heavy and heavy nuclei, where all nucleons vibrate coherently.

In conclusion, there are two possible isoscalar monopole oscillations in the FMD dynamics of an excited  $^{12}\text{C}$  nucleus: (1) cluster moving and (2) cluster breathing. This result is not unique for  $^{12}\text{C}$ , but it is also found for  $^{16}\text{O}$ . The cluster-originated vibration modes are systematically found for all light nuclei that in the framework of the AMD and FMD model exhibit a pronounced cluster component. Vibration (1) finds its natural prolongation at high amplitude in the phenomenon of direct cluster breakup, which is systematically observed in our calculation at very high excitation energy out of the linear response regime.

$\hbar\omega$ (MeV)	initial state (11)		initial state (12)	
	SLy4	SIH	SLy4	SIH
$^{12}\text{C}$	24.2	30.4	20.2 & 24.2	20.8 & 30.7
$^{16}\text{O}$	26.1	32.4	26.2 & 26.8	26.8 & 32.8
$^{40}\text{Ca}$	22.1	27.6	20.9	27.5

TABLE III: Energy of the collective resonances  $\hbar\omega$  recognized as peaks of the spectral function  $\text{FT}[r](\omega)$  obtained by FMD for different selected light nuclei ( $^{12}\text{C}$ ,  $^{16}\text{O}$ , and  $^{40}\text{Ca}$ ) and effective interactions (SLy4, SIH, and Gogny) in the low-amplitude limit with two different initial states.

Table III shows the summary of the peak frequencies  $\hbar\omega$  in the spectral function  $\text{FT}[r](\omega)$  obtained by FMD for different selected nuclei and effective interactions in the small-amplitude limit with different initial excitations. We can see that both the cluster moving and cluster breathing modes are excited when the initial state is prepared by a radial translation of the wave



packets' centroids [Eq. (12)], whereas only the cluster breathing mode is observed if the standard monopole boost [Eq. (11)] is applied to the ground state FMD wave function in the small-amplitude limit. This suggests that the cluster moving mode in  $^{12}\text{C}$  may be due to a coupling between the initial excitation [Eq. (12)] applied on a deformed ground state and the monopole mode built on top of it, owing to the nonlinearity of the FMD dynamics at finite amplitude. A similar effect was already reported in TDHF calculations in Ref. [33]. Moreover, in the case of  $^{12}\text{C}$ , the experimental threshold energy for  $3\text{-}\alpha$  breakup is given by  $E^* = 3E_{\text{g.s.}}(\alpha) - E_{\text{g.s.}}(^{12}\text{C}) = 7.3$  MeV which is below the energy associated with the collective frequency of the cluster moving mode of AMD and FMD, even considering the Coulomb barrier, which is expected to be around 2 MeV [13]. The observed vibration appears then more as a virtual diffusion state than as a resonant state. This is however not the case for all cluster moving modes. As an example we show in Fig. 8 the Fourier transform  $\text{FT}[r](\omega)$  of the FMD oscillation in small amplitude for  $^{24}\text{Mg}$ .

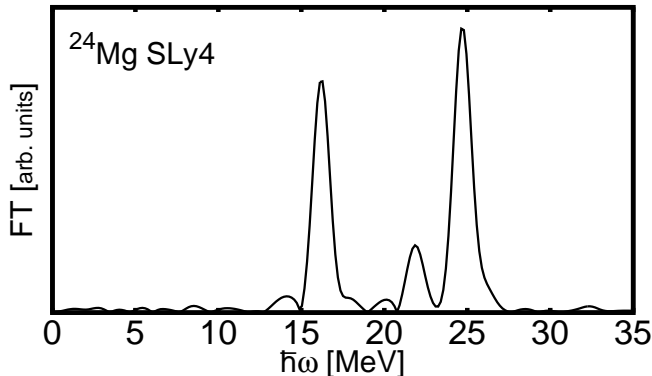


FIG. 8: The spectral function  $\text{FT}[r](\omega)$  in arbitrary units of the FMD monopole oscillation in small amplitude for  $^{24}\text{Mg}$  with the SLy4 interaction.

The ground state of  $^{24}\text{Mg}$  is found to be a deformed prolate shape and it is natural to find a fragmented structure in the spectrum function of such a nucleus since the monopole oscillation is strongly coupled to the quadrupole oscillation. However, the analysis of the variational parameters  $\{a, \vec{b}\}$  reveals that once again the peaks are related to different motions of the underlying quasi-clusters. Specifically, the origin of the three major peaks ( $\hbar\omega = 16, 22$ , and  $25$  MeV) are seen to correspond with  $3\text{"Be"}$ ,  $2\text{"Be"} + 2\text{"}\alpha\text{"}$ , and  $6\text{"}\alpha\text{"}$ , respectively, where "Be" denotes the effective cluster for  $^8\text{Be}$  as " $\alpha$ " for  $^4\text{He}$ . These peak frequencies are below the experimental threshold energy for  $6\text{-}\alpha$  breakup,  $E^* = 6E_{\text{g.s.}}(\alpha) - E_{\text{g.s.}}(^{24}\text{Mg}) = 28.5$  MeV and therefore these resonances may physically exist, although the implementation of the spin-orbit interaction and the projection over angular momentum and parity before the variational procedure will be necessary for a further quanti-

tative discussion.

For comparison, the experimental monopole strength distribution [11] of this nucleus shows a very broad structure peaked at around 21 MeV with a root-mean-square width of around 5-7 MeV, exhausting around 80% of the EWSR. Here again, only qualitative conclusions can be advanced. If the complicated structure of the spectral functions that are systematically observed in light nuclei [8–11] are certainly an indication of a global loss of collectivity, our study suggests that a multiple-peak monopole spectrum can also be an indication of clustered states. A prolongation of this work requires the inclusion of collisions and branching in the molecular dynamics [48], which would allow a quantitative prediction of the strength function as a possible observable to evidence cluster structures.

Other collective modes can also be investigated with our approach by choosing an appropriate initial state and analyzing the associated observable. In fact, in the oscillation calculation of  $^{12}\text{C}$  discussed here, when adopting the initial state (12), we also find another peak around 33 MeV by looking at the Fourier transform of the width variable of a proton wave packet. This extra peak is associated with the isovector monopole mode, which is clearly seen in the Fourier transform of the differential time evolution of the proton and neutron root-mean-square radius ( $R_{\text{proton}} - R_{\text{neutron}}$ ) (the thin line in Fig. 7). Indeed the chosen initial state, where all the wave packets have the same width, contains some isovector excitation in the FMD model because protons and neutrons have slightly different widths in the ground state owing to the Coulomb force.

## VI. SUMMARY

In this paper we have studied collective isoscalar monopole oscillations for some selected light nuclei in the framework of the AMD and FMD time-dependent approaches.

The study of GMR in  $^{40}\text{Ca}$  reveals that for medium-sized nuclei molecular dynamics models are in good agreement with TDHF calculations. A well-defined collective breathing mode is observed at a frequency that depends on the incompressibility modulus of the underlying effective interaction.

Clear collective modes are observed also for nuclei as light as  $^{12}\text{C}$ , but the collective modes in light nuclei appear dominated by quasimolecular cluster structures. We have investigated in great detail the motion of  $^{12}\text{C}$  as an example. The  $^{12}\text{C}$  isoscalar monopole dynamics leads to a spectral function containing two distinct frequencies associated, respectively, with an oscillation of the effective three " $\alpha$ " constituents around the nucleus center of mass and with a coherent vibration of the underlying clusters. This latter frequency sensitively increases with increasing incompressibility of the associated equation of state, but does not follow the empirical  $\propto A^{-1/3}$  law of

the well-known breathing mode in medium-heavy and heavy nuclei. Only the first mode is accessible to AMD calculations, whereas the inclusion of the width degree of freedom appears essential to describe the second one. More complicated spectral functions can be observed in our calculations depending on the cluster structure of the nucleus. The presented calculations do not contain two-body collisions nor quantum branching, meaning that they cannot describe the decay of the observed collective motions, which are expected to considerably increase the fragmentation of the monopole strength. However, the dominant modes should be preserved by such improved calculations [65].

Molecular dynamics calculation such as AMD and FMD therefore will be a powerful tool to study the inter-

play among clustering structures, collective resonances, and multiple breakup of various nuclei in the nuclear chart including unstable nuclei.

### Acknowledgments

This work is supported by the ANR project NExEN (ANR-07-BLAN-0256-02) and by Grant-in-Aid for Scientific Research (KAKENHI) 20-08814 and 21540253 from Japan Society for the Promotion of Science (JSPS). T.F. acknowledges the support from ENSICAEN as post-doctoral fellowship. K. H. O. H also thanks JSPS for his JSPS Postdoctoral Fellowship for Foreign Researchers.

- 
- [1] J. M. Pearson, Phys. Lett. B **271**, 12 (1991).
  - [2] S. Shlomo and D. H. Youngblood, Phys. Rev. **47**, 529 (1993).
  - [3] H. L. Clark, Y. W. Lui, and D. H. Youngblood, Phys. Rev. C **63**, 031301 (2001).
  - [4] D. H. Youngblood, Y. W. Lui, H. L. Clark, B. John, Y. Tokimoto, and X. Chen Phys. Rev. C **69**, 034315 (2004).
  - [5] J. P. Blaizot, Phys. Rep. **64**, 171 (1980), and references therein.
  - [6] S. Shlomo, B. K. Agrawal, and Au V. Kim, Nucl. Phys. **A734**, 589 (2004).
  - [7] G. Colo, N. Van Giai, J. Meyer, K. Bennaceur, and P. Bonche, Phys. Rev. C **70**, 024307 (2004).
  - [8] D. H. Youngblood, Y. W. Lui, and H. L. Clark, Phys. Rev. C **57**, 2748 (1998).
  - [9] B. John et al., Phys. Rev. **68**, 014305 (2003).
  - [10] Y. W. Lui, H. L. Clark, and D. H. Youngblood, Phys. Rev. C **64**, 064308 (2001).
  - [11] D. H. Youngblood, Y. W. Lui, X. F. Chen and H. L. Clark, Phys. Rev. C **80**, 064318 (2009).
  - [12] K. Ikeda, N. Takigawa, and H. Horiuchi, Prog. Theor. Phys. Suppl. **Extra Number**, 464 (1968).
  - [13] T. Yamada and P. Schuck, Phys. Rev. C **69**, 024309 (2004).
  - [14] T. Yamada, Y. Funaki, H. Horiuchi, K. Ikeda, and A. Tohsaki, J. Phys. Conf. Ser. **111**, 012008 (2008).
  - [15] T. Kawabata et al., Phys. Lett. B **646**, 6 (2007).
  - [16] J. Cugnon, Phys. Lett. B **135**, 374 (1984).
  - [17] W. A. Friedman, Phys. Rev. Lett. **60**, 2125 (1988).
  - [18] W. A. Friedman, Phys. Rev. C **42**, 667 (1990).
  - [19] Ph. Chomaz, M. Colonna, and J. Randrup, Phys. Rep. **389**, 263 (2004).
  - [20] V. Viola et al., Phys. Rep. **434**, 1 (2006).
  - [21] B. Borderie, M. F. Rivet, Prog. Part. Nucl. Phys. **61**, 551 (2008).
  - [22] F. Grenier et al., Nucl. Phys **A811**, 233 (2008).
  - [23] A. R. Raduta et al., arXiv:1004.3234.
  - [24] T. Kokalova, N. Itagaki, W. von Oertzen, and C. Wheldon, Phys. Rev. Lett. **96**, 192502 (2006).
  - [25] W. von Oertzen et al., Eur. Phys. Journ. **A 36**, 279 (2008).
  - [26] Ph. Chomaz, N. Van Giai, and S. Stringari, Phys. Lett. B **189**, 375 (1987).
  - [27] N. Van Giai, Ph. Chomaz, P. F. Bortignon, F. Zardi, and R. A. Broglia, Nucl. Phys. **A482**, 437 (2006).
  - [28] P. G. Reinhard, P. D. Stevenson, D. Almed, J. A. Maruhn, and M. R. Strayer, Phys. Rev. E **73**, 036709 (2006).
  - [29] T. Nakatsukasa and K. Yabana, Phys. Rev. C **71**, 024301 (2005).
  - [30] T. Nakatsukasa and K. Yabana, Nucl. Phys. **A788**, 349 (2007).
  - [31] P. D. Stevenson, D. Almed, P. G. Reinhard, and J. A. Maruhn, Nucl. Phys. **A788**, 343 (2007).
  - [32] B. Avez, C. Simenel and Ph. Chomaz, Phys.Rev.C **78**, 044318 (2008).
  - [33] C. Simenel and Ph. Chomaz, Phys.Rev.C **68**, 024302 (2003).
  - [34] C. Simenel and Ph. Chomaz, Phys.Rev.C **80**, 064309 (2009).
  - [35] A. Smerzi, A. Bonasera, and M. Di Toro, Phys. Rev. C **44**, 1713 (1991).
  - [36] E. B. Balbutsev and P. Schuck, Nucl. Phys. **A652**, 221 (1999).
  - [37] E. B. Balbutsev and P. Schuck, Ann. Phys. (NY) **322**, 489 (2007).
  - [38] T. Gaitanos, A. B. Larionov, H. Lenske and U. Mosel Phys. Rev. C **81**, 054316 (2010).
  - [39] S. Drożdż, J. Okolowcz and M. Ploszajczak Phys. Lett. B **109**, 145 (1982).
  - [40] E. Caurier, B. Grammaticos and T. Sami Phys. Lett. B **109**, 150 (1982).
  - [41] W. Bauhoff, E. Caurier, B. Grammaticos and M. Ploszajczak Phys. Rev. C **32**, 1915 (1985).
  - [42] A. Ono, H. Horiuchi, T. Maruyama, and A. Ohnishi, Phys. Rev. Lett. **68**, 2898 (1992).
  - [43] A. Ono, H. Horiuchi, T. Maruyama, and A. Ohnishi, Prog. Theor. Phys. **87**, 1185 (1992).
  - [44] H. Feldmeier, Nucl. Phys. **A515**, 147 (1990).
  - [45] Y. Kanada-En'yo, H. Horiuchi, and A. Doté, Phys. Rev. C **60**, 064304 (1999), and references therein.
  - [46] Y. Kanada-En'yo Phys. Rev. C **75**, 024302 (2007).
  - [47] H. Feldmeier, K. Bieler, and J. Schnack, Nucl. Phys. **A586**, 493 (1995).
  - [48] A. Ono and H. Horiuchi, Prog. Part. Nucl. Phys. **53**, 501

- (2004).
- [49] Y. Kanada-En'yo and M. Kimura, Phys. Rev. C **72**, 064301 (2005).
  - [50] A. Ono and H. Horiuchi, Phys. Rev. C **53**, 2958 (1996).
  - [51] P. Ring and P. Schuck, *The nuclear many-body problem*, (Springer-Verlag, New-York, 1980).
  - [52] P. Bonche, H. Flocard, and P. H. Heenen, Comp. Phys. Commun. **171**, 49 (2005).
  - [53] E. Chabanat, P. Bonche, P. Haensel, J. Meyer, and R. Schaeffer, Nucl. Phys. **A635**, 231 (1998).
  - [54] J. Dechargé and D. Gogny, Phys. Rev. C **21**, 1568 (1980).
  - [55] M. Beiner, H. Flocard, N. Van Giai, and P. Quentin, Nucl. Phys. **A238**, 29 (1975).
  - [56] G. Audi and A. H. Wapstra, Nucl. Phys. **A729**, 337 (2003).
  - [57] T. Neff and H. Feldmeier, Nucl. Phys. **A738**, 357 (2004).
  - [58] T. Neff, H. Feldmeier, and R. Roth, Nucl. Phys. **A752**, 321 (2005).
  - [59] M. Chernykh, H. Feldmeier, T. Neff, P. von Neumann-Cosel, and A. Richter, Phys. Rev. Lett. **98**, 032501 (2007).
  - [60] Y. Kanada-En'yo, Phys. Rev. C **71**, 014310 (2005), and references therein.
  - [61] S. Chikazumi, T. Maruyama, S. Chiba, K. Niita, and A. Iwamoto, Phys. Rev. C **63**, 024602 (2001).
  - [62] S. Stringari and D. Vautherin, Phys. Lett. B **88**, 1 (1979).
  - [63] J. M. Pacheco, E. Maglione, and R. A. Broglia, Phys. Rev. C **37**, 2257 (1988).
  - [64] G. Colo, P. F. Bortignon, S. Fracasso, and N. Van Giai, Nucl. Phys. **A788**, 173 (2007).
  - [65] G. Colo, P. F. Bortignon, N. Van Giai, A. Bracco, and R. A. Broglia, Phys. Lett. B **276**, 279 (1992).